Ocean Sci. Discuss., 10, 1031–1065, 2013
www.ocean-sci-discuss.net/10/1031/2013/
doi:10.5194/osd-10-1031-2013

Ocean Science
Discussions
Open Access

Equilibrator-based measurements of dissolved nitrous oxide in the surface ocean using an integrated cavity output laser absorption spectrometer

I. Grefe and J. Kaiser

School of Environmental Sciences, University of East Anglia, Norwich Research Park, Norwich, UK

Received: 28 May 2013 – Accepted: 10 June 2013 – Published: 3 July 2013

Correspondence to: J. Kaiser (j.kaiser@uea.ac.uk)

Published by Copernicus Publications on behalf of the European Geosciences Union.

Abstract

A laser-based analyser for nitrous oxide, carbon monoxide and water vapour was coupled to an equilibrator for continuous high-resolution dissolved gas measurements in the surface ocean. Results for nitrous oxide measurements from laboratory tests and field deployments are presented here. Short-term precision for 10 s-average N_2O mole fractions at an acquisition rate of 1 Hz was better than 0.2 nmol mol^{-1} for standard gases and equilibrator measurements. The same precision was achieved for replicate standard gas analyses within 1 h of each other. The accuracy of the equilibrator measurements was verified by comparison with purge-and-trap GC-MS measurements of N_2O concentrations in discrete samples from the Southern Ocean and showed agreement to within the 2 % measurement uncertainty of the GC-MS method. Measured atmospheric N_2O mole fractions agreed with AGAGE values to within 0.4 %. The equilibrator response time to concentration changes in water was 142 to 203 s, depending on the headspace flow rate. The system was tested at sea during a north-to-south transect of the Atlantic Ocean. While the subtropical gyres were slightly undersaturated, the equatorial region was a source of nitrous oxide to the atmosphere. The ability to measure at high temporal and spatial resolution revealed sub-mesoscale variability in dissolved N_2O concentrations. The magnitude of the observed saturation is in agreement with published data. Mean sea-to-air fluxes in the tropical and subtropical Atlantic ranged between −1.6 and 0.11 µmol m^{-2} d^{-1} and confirm that the subtropical Atlantic is not an important source region for N_2O to the atmosphere, compared to average global fluxes of 0.6 to 2.4 µmol m^{-2} d^{-1}. The system can be easily modified for autonomous operation on voluntary observing ships (VOS). Further work should include an inter-laboratory comparison exercise with other methods of dissolved N_2O analyses.

OSD
10, 1031–1065, 2013

1 Introduction

Nitrous oxide (N_2O) is an important trace gas in the atmosphere, influencing earth's climate as well as stratospheric chemistry. It is currently the third most important greenhouse gas in terms of 100 a global warming potential after CO_2 and CH_4 (Ravishankara et al., 2009). Furthermore, it is the main precursor of stratospheric NO_x, which catalytically destroys ozone (Crutzen, 1970). As CFCs are phased out under the Montreal Protocol, N_2O is the most important, currently emitted substance involved in stratospheric ozone depletion (Ravishankara et al., 2009). Atmospheric concentrations are rising at a rate of $0.26\,\%\,a^{-1}$ with the ocean contributing about 30 % to total emissions (Forster et al., 2007). Bacterial nitrification and denitrification are assumed to be the main production pathways for N_2O in the ocean, while denitrification can also act as a sink under suboxic conditions (Elkins et al., 1978; Cohen and Gordon, 1978; Knowles, 1982). Even though nitrification is an aerobic process, N_2O production is enhanced as oxygen concentrations decrease (Goreau et al., 1980; Yoshida et al., 1989; Yoshinari, 1976). Nitrifier-denitrification is an alternative pathway for N_2O production by ammonia oxidising bacteria, which appears to be important for the near-surface N_2O source (Poth and Focht, 1985; Popp et al., 2002; Sutka et al., 2004, 2006). Recently, the importance of N_2O production by archaeal ammonia oxidation was discovered, potentially accounting for a significant part of the oceanic N_2O source (Löscher et al., 2012; Wuchter et al., 2006). The estimated source of rivers and coastal regions range currently from 0.5 to $2.7\,Tg\,a^{-1}$ (in N equivalents) and from 1.8 to $5.8\,Tg\,a^{-1}$ for the open ocean (Denman et al., 2007). In the light of the uncertainties in the marine N_2O source and potential future emission increases due to ocean deoxygenation (Codispoti, 2010), accurate observations in space and time are important to give a better estimate of regional sources and global budgets.

The most common technique for N_2O concentration measurements is injection of a gas sample onto a gas chromatographic column coupled to an electron capture detector (GC-ECD) (Weiss et al., 1992; Butler et al., 1989). Here we present an alternative

OSD
10, 1031–1065, 2013

method using a laser-based optical absorption analyser (Baer et al., 2002) that in combination with an equilibrator enables continuous N_2O analyses at ambient levels in seawater. The system is low-maintenance, can be easily calibrated and allows for higher measurement frequency than GC-ECD methods. It has the potential to facilitate observations over long time series, revealing variability and trends, as is already happening for CO_2 measurement systems, e.g. on ships of opportunity. Laboratory tests and results from field deployments of the analyser in combination with an equilibrator are presented.

2 Materials and methods

2.1 Laboratory tests

The N_2O/CO analyser (Los Gatos Research, LGR, model N_2O/CO-23d), used in this study, measures mole fractions of N_2O, carbon monoxide (CO) and water vapour (H_2O) using off-axis integrated cavity output spectroscopy (ICOS). Test results and environmental data for N_2O are reported in this study. The analyser was connected to a 1.7 L percolating packed glass bed equilibrator as described by Cooper et al. (1998). The analyser's internal membrane pump was used to circulate the gas phase through the equilibrator. Water was pumped through the equilibrator at a flow rate of 1.8 L min^{-1}. Two 4-port 2-position valves (Vici) allowed for fast switching between the equilibrator headspace and a 6-port multi-position valve (Vici), connecting to other gas lines e.g. atmospheric air and references (Fig. 1). A similar setup has been described by Gülzow et al. (2011) for dissolved CO_2 and CH_4 measurements using an ICOS analyser and by Becker et al. (2012) for measurements of ffi$^{13}C(CO_2)$ and fCO_2 using continuous wave cavity ringdown spectroscopy.

A water trap was installed downstream of the equilibrator to reduce the amount of water vapour in the headspace gas. The trap consisted of a thermoelectric cool box (T08 DC, Mobicool), held at 5 °C, and a miniature filter with manual drain (Norgren)

OSD
10, 1031–1065, 2013

to collect the condensing water. A custom-built safety valve ("water guard") was installed upstream of the analyser as an additional protection against water entering the measurement cell. The water guard consists of a stainless steel tee (Swagelok) with electrodes and a solenoid valve downstream of the sensor. Water in the gas line closes the electric circuit in the water guard, triggering the closure of the valve and cutting off the gas supply to the analyser. This is really just a safety precaution as the "water-guard" was neither triggered during the laboratory tests, nor at sea. The instrument's water vapour measurements are used by the software to calculate N_2O dry mole fractions (Eq. 1). $x(N_2O)$ is the N_2O dry mole fraction, $x_{meas}(N_2O)$ and $x_{meas}(H_2O)$ are the measured N_2O and H_2O mole fractions:

$$x(N_2O) = \frac{x_{meas}(N_2O)}{1 - x_{meas}(H_2O)} \quad (1)$$

Furthermore, line broadening due to changing water vapour concentrations is accounted for by the instrument's software. In order to validate this water vapour correction, measurements of dry air were compared to calculated values for the dry mole fraction of humidified air. A cylinder with dry air was connected to the analyser via the multi-position valve. The gas line from the cylinder was split with one line going directly to the valve and the other one passing first through the water-filled cold trap to humidify the air. H_2O mole fractions were between 1 and 1.4 % for the humidified gas and below the analyser's detection limit (around 0.2 % for H_2O) for dry gas. The calculated dry mole fraction of the humidified gas was compared to that of the dry gas.

In addition, to test for analyser variability and drift, dry cylinder gas was measured for 24 h. To test for leaks within the analyser, laboratory air (325 nmol mol^{-1} dry mole fraction, uncalibrated) and zero grade air (O_2 and N_2, 84 nmol mol^{-1} N_2O dry mole fraction uncalibrated, BOC) were mixed in a sample loop to obtain lower mole fractions than in ambient air. The mixtures with 215.1 nmol mol^{-1} N_2O were re-circulated through the analyser for 12 and 21 min. Any leaks are expected to be noticed as an increase in N_2O mole fractions caused by ambient air. The valve board was leak-checked separately by pressurising the gas lines of the equilibrator loop with compressed air to just

OSD
10, 1031–1065, 2013

below 120 kPa. The equilibrator itself was bypassed as it would vent to the atmosphere through the pressure vent and the flow-through water line. As the LGR analyser keeps the pressure in the measurement cell constant at 100 kPa, a Licor CO_2 instrument with built-in pressure gauge was used instead for monitoring pressure changes over time.

The response time of the coupled system of ICOS analyser and equilibrator was characterised in further laboratory tests. The equilibrator time constant τ, i.e. the time during which a concentration difference between the gas- and the water phase declines to $1/e$ (36.8 %) with regard to the start value, was determined as described in Gülzow et al. (2011). τ was only evaluated for N_2O as CO background concentrations were too variable in the laboratory where tests took place. Two 100 L reservoirs, open to the atmosphere, were filled with fresh water from the mains, which is supersaturated in N_2O. Mole fractions between 694 and 1065 nmol mol^{-1} were measured in the equilibrator headspace during five experiments with supersaturated water. One of the reservoirs was then equilibrated with ambient air by re-circulation; the other was kept at elevated N_2O concentrations. For the experiments, the water was pumped through the equilibrator from the bottom of the reservoirs at a flow rate of 1.8 L min^{-1}, starting with the equilibrated reservoir, and then changing to water with high N_2O concentrations. After the measured dry mole fraction reached a plateau (x_{max}), water in equilibrium with ambient air was pumped through the equilibrator. τ was then calculated as described in Gülzow et al. (2011), recording the decay of N_2O dry mole fractions (x_t) back to ambient values (x_{min}). The observed x_t values (Fig. 2) were fitted to an exponential equation:

$$x_t = x_{min} + (x_{max} - x_{min})e^{\frac{-t}{\tau}} \quad (2)$$

By rearranging Eq. (2), τ can be inferred from the slope of $-\ln[(x_t - x_{min})/(x_{max} - x_{min})]$ over time.

Initially, it was attempted to use the analyser in combination with a semi-permeable membrane (Membrana, MiniModule). For this purpose, the gas flow through the cavity was reduced to 100 mL min^{-1} (293 K, 100 kPa) by inserting a needle valve between

OSD
10, 1031–1065, 2013

the internal diaphragm pump and a check valve downstream the measurement cell. The yield of dissolved gases extracted over the membrane was too low to sustain the analyser's operating pressure in the measurement cell. Therefore, an equilibrator was used instead of the semi-permeable membrane. As the reduced gas flow did not lead to problems with the equilibrator setup, the valve was retained during the first field test (see Sect. 2.2). Without the throttle valve, the flow rate increased to approximately 400 mL min^{-1} (293 K, 100 kPa). The time constant τ was determined for both headspace flow rates.

2.2 Field deployment

The N_2O analyser was tested at sea during cruise AMT20 of the Atlantic Meridional Transect project from Southampton, UK to Punta Arenas, Chile (12 October to 25 November 2010) on board RRS James Cook. Figure 3 shows the setup for underway measurements during the cruise, Fig. 4 the cruise track.

The equilibrator was connected to the ship's pumped underway seawater supply, drawing water from a depth of approximately 5 m. Filters (Vacu-guard, part number 6722-5000, Wheaton) were inserted at the gas in- and outlets of the equilibrator to protect pump and measurement cell of the analyser from seawater. Temperatures in the equilibrator were measured with two calibrated Pt-100 temperature probes (Omega Engineering Limited) at a precision of better than 0.1 °C. The water flow through the equilibrator was set to approximately 1.8 L min^{-1} at the tap regulator but was not stable over time and had to be re-adjusted regularly. Changes in the flow could be due to vibration of the ship changing the setting of the regulator on the tap, as well as the varying demand of seawater in other labs on board. For subsequent field deployments, a flow restrictor will be used to stabilise the pumped seawater supply to the equilibrator. Two three-way valves (part number SS-41GXS2, Swagelok) allowed changing between sample gas stream from the equilibrator and marine air, drawn from the ship's bow (Fig. 3). Dried air with 323.7 nmol mol^{-1} was used as a working reference, calibrated against IMECC/NOAA primary standards. Every 8 h, the analyser was calibrated by

OSD
10, 1031–1065, 2013

switching from equilibrator headspace to the reference gas and then marine air for 20 min each. This was followed by another reference measurement after 40 min to assess short-time drift. Only the last 5 min of each measurement were analysed to allow for complete flushing of the measurement cell. Correspondingly, the first 15 min after switching back to the equilibrator headspace or to air measurements were not used for evaluation.

N_2O concentrations (c) were calculated from dry mole fractions (x) using the solubility function F at equilibrator temperature T_{eq} (Weiss and Price, 1980):

$$c = xF(T_{eq}, S)p_{eq} \quad (3)$$

where T_{eq} and p_{eq} are equilibrator temperature and pressure (assumed to be equal to ambient atmospheric pressure, p_{air} at sea level and assuming 100 % relative humidity) and S is salinity. Seawater saturations (s) were based on equilibrium values for measured atmospheric mole fractions x_{air} and mole fractions in seawater, corrected for temperature differences between equilibrator and seawater intake (T_{in}):

$$s = \frac{xF(T_{eq}, S)}{x_{air}F(T_{in}, S)} \quad (4)$$

The air-sea flux (Φ) was calculated from the gas transfer coefficient (k_w) and the difference between N_2O concentrations in seawater c and air equilibrium concentrations (c_{air}):

$$\Phi = k_w(c - c_{air}) = k_w[c - x_{air}F(T_{in}, S)p_{air}] \quad (5)$$

k_w was calculated using the parameterisation of Nightingale (2000) and converted to units of $m\,d^{-1}$, where u is wind speed at 10 (Eq. 6). This relationship shows an intermediate dependence on wind speed compared to the other frequently used parameterisations of Liss and Merlivat (1986) and Wanninkhof (1992). k_w was adjusted for N_2O with the Schmidt number Sc calculated following Wanninkhof

OSD
10, 1031–1065, 2013

(1992). The wind speed was taken from the 6 hourly operational analysis dataset of the European Centre for Medium-Range Weather Forecasts and interpolated to the time and position of the respective measurement (ECMWF, available from http://badc.nerc.ac.uk/view/badc.nerc.ac.uk__ATOM__dataent_ECMWF-OP).

$$\frac{k_w}{\mathrm{m\,d^{-1}}} = 0.24\left[0.222\left(\frac{u}{\mathrm{m\,s^{-1}}}\right)^2 + 0.333\left(\frac{u}{\mathrm{m\,s^{-1}}}\right)^2\right]\left(\frac{\mathrm{Sc}}{600}\right)^{-0.5} \quad (6)$$

Instantaneous values for k_w and Φ were compared to those using 30 day-wind speed-weighted averages (Reuer et al., 2007). Differences between both estimates of sea-air exchange were small. In the following, we discuss only instantaneous fluxes for consistency with previous studies of N_2O air-sea exchange (Fig. 5).

In addition to the data from AMT20, we also present reference gas and atmospheric measurements, as well as a comparison with discrete samples from a subsequent cruise to the Weddell Sea on board RRS James Clark Ross from 20 January to 2 February 2012 (JR255A) in Sect. 3.2. The majority of the sea surface measurements on this cruise will be discussed elsewhere, but we have included results from a comparison of equilibrator-ICOS measurements with GC-MS data.

2.3 GC-MS measurements

During AMT20, no discrete field measurements are available for comparison with the analyser measurements. During a subsequent deployment of the equilibrator-ICOS system in the Weddell Sea, three CTD samples were collected and analysed for N_2O concentrations using purge-and-trap Gas Chromatography-Isotope Ratio Mass Spectrometry (GC-IRMS) measurements of surface CTD samples is compared to the analyser data.

CTD seawater samples for isotope analysis were collected in 500 mL (nominal value) serum bottles (Wheaton). Triplicate samples were taken immediately after recovery of the CTD and were allowed to overflow at least three times the bottle volume. Sample bottles were closed with butyl stoppers and aluminium crimp seals and poisoned

OSD
10, 1031–1065, 2013

with 1 mL saturated mercuric chloride solution. 1 mL of the sample was replaced with CP grade helium (BOC) to reduce the risk of leaks due to temperature driven volume changes of the water during transport and storage. The setup of the GC-MS setup follows McIlvin and Casciotti (2010). Samples are loaded manually; dissolved gases are quantitatively extracted with a helium purge stream and trapped with liquid nitrogen. Water vapour in the gas stream is removed with a Nafion dryer (Perma Pure), CO_2 is trapped on Carbosorb (Merck). The sample is then injected into a continuous-flow GC-MS system. Late eluting substances are removed with a pre-column as described in Röckmann et al. (2003) before N_2O is separated from residual CO_2 on the PoraPlot Q analytical column. The sample enters the mass spectrometer (Thermo Scientific, MAT 253) via an open split and is analysed for mass-to-charge ratios 44, 45 and 46, as well as peak area. The N_2O concentration in the sample can be calculated from the peak area with a precision of 2 % and the sample volume, which is determined by sample weight, water temperature and salinity, with a precision of 0.02 %. The overall precision of 2 % is comparable to the 1.8 % concentration uncertainty achieved for GC-ECD measurements by Walter et al. (2006) and 2.6 % for GC-MS measurements by McIlvin and Casciotti (2010).

3 Results and discussion

3.1 Laboratory tests

To improve the precision of individual data points retained for further analysis, 10 s averages were calculated from measurements at 1 Hz. Since the headspace gas was in contact with the water phase in the equilibrator, water vapour concentrations were high. The cold trap only removed water to a dew point of 5 °C. Correction from measured values to dry mole fractions is therefore required for the evaluation of dissolved N_2O concentrations in seawater.

OSD
10, 1031–1065, 2013

Compressed air directly from the cylinder had a measured N_2O mole fraction of $(332.7 \pm 0.2)\,\mathrm{nmol\,mol^{-1}}$, while H_2O mole fractions were below the detection limit of 0.2 %. The measured N_2O mole fraction in humidified air with $10.6\,\mathrm{mmol\,mol^{-1}}$ H_2O was $(329.7 \pm 0.2)\,\mathrm{nmol\,mol^{-1}}$. Since the H_2O mole fraction in compressed air was below the detection limit of 0.2 %, we assume it to be in the range from 0 to 0.2 %. The corresponding dry mole fraction of compressed air is therefore $(332.7^{+0.8}_{-0.2})\,\mathrm{nmol\,mol^{-1}}$, where the error estimate in the positive direction corresponds to a H_2O mole fraction of 0.2 %, that in the negative direction corresponds to the statistical uncertainty and a H_2O mole fraction of 0 %. The calculated dry mole fraction of humidified air was $(333.1 \pm 0.2)\,\mathrm{nmol\,mol^{-1}}$. This value is within measurement uncertainties of the corrected mole fraction of compressed air directly from the cylinder. The H_2O vapour dilution correction is considered to be sufficient; no further corrections for line broadening were applied.

The stability of the analyser at low N_2O mole fractions was assessed by measuring a gas cylinder over 24 h. The standard deviation was $0.2\,\mathrm{nmol\,mol^{-1}}$ for a mean N_2O mole fraction on $48.7\,\mathrm{nmol\,mol^{-1}}$. Minimum- and maximum values measured during this period were 48.2 and $49.4\,\mathrm{nmol\,mol^{-1}}$ respectively.

The highest observed increase of N_2O mole fractions during the two leak tests for the LGR analyser was $0.024\,\mathrm{nmol\,mol^{-1}\,min^{-1}}$. The gas volume of the 400 mL measurements cell at a pressure of 100 kPa corresponds to 40 mL while the tubing of the circular gas path for this test is assumed to be at atmospheric pressure, resulting in a volume of approximately 40 mL. The total gas volume during the test is therefore 80 mL The leak rate was calculated as the increase in N_2O concentrations, divided by the difference between background N_2O and circulating gas mixture and multiplied by the total gas volume. The resulting leak rate for the N_2O analyser used for re-circulating air, e.g. through an equilibrator, is $0.017\,\mathrm{mL\,min^{-1}}$ or $0.29 \times 10^{-3}\,\mathrm{mL\,s^{-1}}$. This leak rate is likely to be due to the pump head (on the order of $10^{-3}\,\mathrm{mL\,s^{-1}}$, KNF Neuberger (UK) Ltd, personal communication, 2013). Pressure in the valve board was stable over 10 min at $119\,731 \pm 0.006$ Pa as recorded by the Licor's pressure gauge, indicating the absence of leaks.

OSD
10, 1031–1065, 2013

The response time of the coupled analyser-equilibrator system to concentration changes in the water phase is described by the equilibration time constant τ. For a gas flow of 400 mL min^{-1} through the measurement cell, τ equalled (142 ± 1) s for N_2O (n = 5). The 95 % relaxation time (= 3t) is therefore about 7 min. Reducing the gas flow to 100 mL min^{-1} increased t to (203 ± 1) s (n = 3). In the limit where the water flow rate is much higher than the gas exchange rate, the value for t depends on the transfer coefficient k (Rafelski et al., 2012). Presumably, at the higher gas flow rate enhanced turbulence increased the efficiency of gas transfer between water and gas. Therefore, the needle valve will be removed during future deployments to reduce delays in the system's response to changing N_2O concentrations in the environment.

3.2 Precision and accuracy

Under field conditions during AMT20, the difference between two subsequent calibration measurements, spaced 40 min apart, was on average 0.2 nmol mol^{-1} or better. Over the course of the field campaign, substantial long-term drift was encountered as discussed in Sect. 3.3. As this drift was due to a faulty laser and not the measurement system itself, it is not further discussed in this section. After the replacement of the laser, the analyser was used during a research cruise in the Weddell Sea (JR255A). Three reference gases were used and precision for corrected dry mole fraction values over the length of the field campaign was 0.9 nmol mol^{-1} (0.3 %) or better for all three gases (n = 19).

Measurements of atmospheric N_2O mole fractions during AMT20 and JR255A were used for comparison with data of selected Advanced Global Atmospheric Gases Experiment (AGAGE) stations (Prinn et al., 2000). Dry mole fractions were corrected for instrument drift and offset with the calibration measurements. During AMT20, mole fractions of N_2O measured in marine background air were (323.2 ± 0.5) nmol mol^{-1} throughout the cruise. An interhemispheric difference of slightly less than 1 nmol mol^{-1} was expected (Butler et al., 1989; Rhee et al., 2009), but did not show in the data. This small difference might have not been captured due to the analyser drift described

OSD
10, 1031–1065, 2013

below. The measured atmospheric mole fractions of $(325.2 \pm 0.5)\,\mathrm{nmol\,mol^{-1}}$ agree within measurement uncertainties with mean values for October and November of the AGAGE stations Mace Head for the Northern Hemisphere ($(324.1 \pm 0.7)\,\mathrm{nmol\,mol^{-1}}$) and Cape Grim for the Southern Hemisphere ($(322.9 \pm 0.3)\,\mathrm{nmol\,mol^{-1}}$, data from http://agage.eas.gatech.edu/data_archive) (Fig. 6). During JR255A, measured N_2O mole fractions in air were $(323.9 \pm 1.3)\,\mathrm{nmol\,mol^{-1}}$ ($n = 11$), which is consistent with the value of $(323.9 \pm 0.5)\,\mathrm{nmol\,mol^{-1}}$ measured at Cape Grim in January 2012. The slightly poorer precision for air measurements in the Weddell Sea might be due to the position of the air intake. On board the RRS James Cook the inlet was located at the bow of the ship, while air was drawn from the starboard side of the bridge on the RRS James Clark Ross. Traces of the ship's exhaust might have entered the measurement line at times, leading to more variable results. However, the measurement uncertainty for JR255A is on the order of 0.4 % and therefore still very good.

The equilibrator type used for seawater measurements is described in Cooper et al. (1998). The authors found no systematic differences for CO_2 measurements made with this equilibrator compared to shower-head equilibrators. As the solubility characteristics of N_2O are similar to CO_2 (Weiss and Price, 1980), no bias is expected to be introduced by using this equilibrator type and the equilibrator efficiency should be similar.

Discrete water samples for N_2O isotope measurements were collected during JR255A. Three depth casts were overlapping with the analyser data and concentration in surface samples are compared to the on-line data (Table 1).

Concentrations measured with GC-MS were (1.3 ± 0.9) % higher than those obtained with the LGR N_2O analyser. Although the values are still overlapping in terms of the 2 % measurement uncertainty associated with the GC-MS measurements, this could point towards laboratory air being drawn into the equilibrator through the vent. Another potential explanation could be the consumption of N_2O in anoxic biofilms within the ship's seawater pipes (Juranek et al., 2010). In future, GC-MS or GC-ECD samples

OSD
10, 1031–1065, 2013

from the pumped seawater supply should be compared with analyser and CTD data to resolve the origin of the small offset between the two methods.

3.3 AMT20 results

The coupled system of N_2O analyser and equilibrator was tested in the field for the first time during AMT20 in boreal autumn 2010. The system worked well initially, but two problems occurred: (1) it was difficult to keep the water flow through the equilibrator constant (see Sect. 2.2), which led to pressure variations in the equilibrator and spurious results; (2) the measured values for the N_2O reference gas drifted (Fig. 7).

Short-term drift was negligible, though, as discussed in Sect. 3.2. Therefore, the reference gas measurements could be used to fully correct air and equilibrator measurements for analyser offset and drift, using linear interpolation between calibrations (see also Fig. 6). The instrument drift was caused by a gradual change of the laser tuning (R. Provencal, personal communication, 2010), The laser was replaced after AMT20 and the analyser has been stable since.

Measurements of dissolved N_2O in the surface ocean were collected between 24° N and 39° S. Due to the problems with the laser no data was collected between 4° N and 2° S and between 5 and 14° S (Fig. 4). N_2O concentrations in surface waters ranged from 5.5 to 8.6 nmol L^{-1}, with lowest average concentrations measured in the North Atlantic Gyre between 24 and 11° N (Fig. 8, Table 2). Surface waters were slightly undersaturated. However, towards the southern limb of the gyre, an increase in N_2O saturations above mean values of 99.0 % were observed on three occasions between 20 and 11° N. These periods lasted 14, 4 and 12 h respectively, while saturations increased to up to 104 % (Fig. 9b, arrows).

Potential sources for N_2O could be entrainment of deep waters into the mixed layer or advection from the oxygen minimum zone of the Mauritanian upwelling. Another potential source could be in situ production by nitrification or nitrifier-denitrification. High rates of nitrogen fixation were previously observed in this region (Moore et al., 2009) and could provide a substrate for N_2O producing bacteria. Forster et al. (2009)

OSD
10, 1031–1065, 2013

found average saturations of 104 % during spring but 97 % saturation during autumn in the latitude band between 26 and 11° N, comparable to the 99 % mean saturation measured in autumn for this study. More data are needed to confirm whether there is a real seasonal trend towards lower N_2O saturations in the North Atlantic Gyre during boreal autumn.

Highest saturations of up to 107 % were found close to the equator. However, average saturations for the equatorial region between 11° N and 5° S were only 100.4 %. Surface saturations of 104–109 % on average were previously reported for this region (Walter et al., 2004; Forster et al., 2009; Oudot et al., 2002). Rhee et al. (2009) found maximum saturations of 110 % at the equator. Unfortunately, no data could be collected directly at the equator, due to analyser maintenance between 5° N and 2° S. High surface saturations can be expected due to equatorial upwelling of N_2O-rich waters. N_2O saturations of 99.3 % and the lowest N_2O concentrations were measured between 10.6–5.8° N and 27.5–31.5° W, associated with low salinities. Walter et al. (2004) observed similarly low saturations of about 100 % in this region and related it to a retroflection of the North Brazil Current, advecting low-salinity Amazon plume waters into the North Equatorial Counter Current (NECC).

N_2O concentrations increased south of 14° S and reached mean values of 7.7 nmol L^{-1} between 25 and 39° S. While surface waters in the latitudinal band of 14–25° S were on average in equilibrium with the atmosphere, saturations decreased south of 25° S (Fig. 9b) as water temperature decreased. Mean saturations between 14 and 39° S were 99.7 %, similar to 101 % saturation observed in austral spring (Forster et al., 2009; Rhee et al., 2009), while average saturations in austral autumn were higher (104 %, Forster et al., 2009) This was attributed to accumulated N_2O production during spring and summer.

Eddies can bring thermocline waters with higher nutrient and N_2O concentrations into the mixed layer (McGillicuddy et al., 2007). This might stimulate in situ N_2O production from remineralisation of additional biomass as well as increase the mixed layer inventory simply due to mixing with deeper waters with higher

OSD
10, 1031–1065, 2013

N_2O concentrations. Satellite altimeter products from Ssalto/Duacs (gridded sea level anomalies, $1/3^\circ \times 1/3^\circ$ grid, http://www.aviso.oceanobs.com/en/data/products/sea-surface-height-products/global.html) were used to trace eddies. No clear relationship between sea level anomalies (SLA) and saturations was observed in the northern gyre (Fig. 10). Between 28 and 36° S, however, higher N_2O saturations seem to be associated with negative SLAs, while lower saturations occur with positive SLAs. This could point towards upwelling eddies, introducing waters with higher N_2O concentrations, possibly originating from the Benguela upwelling, to the South Atlantic gyre region.

Generally, oligotrophic gyres are expected to be weak N_2O sinks, especially in winter, due to thermal effects, with a potential for weak sources in summer while coastal and equatorial upwelling zones are sources of N_2O (Nevison et al., 1995; Suntharalingam and Sarmiento, 2000). The gyres in both hemispheres were acting as sinks for atmospheric N_2O at the time of the survey, due to slightly undersaturated surface waters (Fig. 9a). Average fluxes for the region between 24–11° N were $(-0.14 \pm 0.31)\,\mu mol\,m^{-2}\,d^{-1}$ and $(-0.16 \pm 0.33)\,\mu mol\,m^{-2}\,d^{-1}$ for 14–39° S (Table 2). For comparison, Forster et al. (2009) observed negative sea-to-air N_2O fluxes between -0.02 and $-0.04\,\mu mol\,m^{-2}\,d^{-1}$ between 26 and 11° N during autumn, corresponding to weak N_2O uptake. Fluxes in spring were positive. The southern gyre was found to be a source of N_2O at all times. They pointed out, that emissions in spring were four times higher between 6–40° S than in autumn, rather due to varying N_2O inventories in the mixed layer than to changing wind speeds. This points towards remarkable inter-annual differences in the oceanic N_2O source and, as shown in this study, also intra-annual variation.

The equatorial region was a source of N_2O to the atmosphere where high surface saturations coincided with relatively high wind speeds. The average flux was $(0.53\,\mu mol\,m^{-2}\,d^{-1}$ between 10° and 3° N, which is most likely an underestimation, due to analyser downtime. Comparable values of $0.52\,\mu mol\,m^{-2}\,d^{-1}$ for the latitudinal band between 12–1.5° N (Walter et al., 2004). For latitudes between 11° N and 5° S, the

OSD
10, 1031–1065, 2013

Western Tropical Atlantic Longhurst province, emissions of $(0.11 \pm 0.26)\,\mu mol\,m^{-2}\,d^{-1}$ were measured. For comparison, $0.16–0.33\,\mu mol\,m^{-2}\,d^{-1}$, were previously reported from the Atlantic Ocean during austral spring (Forster et al., 2009). There might be seasonal variability, as higher emissions were observed during austral autumn ($1.17–2.13\,\mu mol\,m^{-2}\,d^{-1}$, Forster et al., 2009).

Generally, saturations reported here are within the lower range of previously published values for the tropical and subtropical Atlantic which might be due to N_2O consumption in anoxic biofilms within the pumped seawater system as discussed above.

4 Summary and conclusions

Laboratory and field test showed that the Los Gatos N_2O/CO analyser can be coupled with an equilibrator to reliably measure both, atmospheric and marine N_2O concentrations. Small-scale changes of concentrations could be observed, giving a very detailed picture of the marine N_2O budget. This is important for monitoring environments that are highly variable in space and time.

The system is virtually ready for deployment on platforms of opportunity as shown for a similar setup for methane and carbon dioxide measurements (Gülzow et al., 2011). It records high-resolution data while operation is low maintenance and can be easily automated. This is an advantage to labour intensive discrete sampling techniques. Calibration can be automated and atmospheric and marine dissolved gas measurements can be analysed in alternation using the same instrument. The resolution of the described system is good (relaxation time of 140 s for a headspace flow rate of $400\,mL\,min^{-1}$), but response times could be reduced further by increasing the headspace flow, decreasing the headspace volume or, potentially, by decreasing the instrument operating pressure and measurement cell volume. The instrument is protected from water by a cold trap and a solenoid valve connected to a humidity detector. The cold trap currently requires manually draining every 2–3 days, but this could be automated as for CO_2 analysers. Another remaining operator-dependent task is cleaning

OSD
10, 1031–1065, 2013

of the seawater flow regulator, which could be avoided by using screens and pre-filters. However, this is a problem common to all equilibrator techniques. Measurements of depth profiles would require large sample sizes or a pumped CTD due to the relatively long relaxation time of the equilibrator. For depth profiles, headspace sampling would therefore be the preferred option.

The laser drift experienced during AMT20 does not relate to the experimental setup and the instrument has been deployed successfully after laser replacement without further issues. Although no direct GC-ECD measurements were carried out during AMT20, and only few overlapping GC-MS measurements during JR255A, saturation values from measurements with the analyser-equilibrator setup are comparable to previous studies using gas chromatography and the agreement with atmospheric AGAGE measurements is excellent. Although more data points over a wider range of concentrations comparing measurements of the N_2O analyser to other methods would be desirable, this small dataset gives a first indication that the analyser data and the applied corrections result in realistic values for environmental measurements. Further data comparison with GC-ECD measurements in the laboratory and during field campaigns should be implemented in the future. Another interesting test would be comparing the performance of this coupled equilibrator-analyser setup with other equilibrator types and laser-based N_2O analysers of different manufacturers.

Acknowledgements. We would like to thank captain and crew of RRS James Cook and principal scientist Andy Rees for their support during AMT20, as well as BODC for underway sea surface data. Helpful discussions with Grant Forster and Sunke Schmidtko (UEA) are gratefully acknowledged. We would also like to thank Doug Baer and Robert Provencal (Los Gatos Research) for support with the N_2O/CO analyser and Dorothee Bakker for providing the equilibrator used in this study. Special thanks go to Gareth A. Lee for invaluable help with the laboratory experiments and fieldwork preparation. This study was supported by the European Community's Seventh Framework Programme (FP7/2007-2013) under grant agreement number 237890 (Marie Curie Initial Training Network "INTRAMIF") and UK Natural Environment Research Council National Capability funding to Plymouth Marine Laboratory and the National Oceanography Centre, Southampton. This is contribution number 222 of the AMT programme.

OSD
10, 1031–1065, 2013

References

Baer, D. S., Paul, J. B., Gupta, M., and O'Keefe, A.: Sensitive absorption measurements in the near-infrared region using off-axis integrated-cavity-output spectroscopy, Appl. Phys. B Lasers O., 75, 261–265, 2002.

Butler, J. H., Elkins, J. W., Thompson, T. M., and Egan, K. B.: Tropospheric and dissolved N_2O of the west Pacific and east Indian Oceans during the El Nino Southern Oscillation event of 1987, J. Geophys. Res., 94, 14865–14877, 1989.

Codispoti, L. A.: Interesting times for marine N_2O, Science, 327, 1339–1340, doi:10.1126/science.1184945, 2010.

Cohen, Y. and Gordon, L. I.: Nitrous oxide in the oxygen minimum of the eastern tropical North Pacific: evidence for its consumption during denitrification and possible mechanisms for its production, Deep-Sea Res., 25, 509–524, 1978.

Cooper, D. J., Watson, A. J., and Ling, R. D.: Variation of pCO_2 along a North Atlantic shipping route (UK to the Caribbean): a year of automated observations, Marine Chemistry, 60, 147–164, 1998.

Crutzen, P. J.: The influence of nitrogen oxides on the atmospheric ozone content, Q. J. Roy. Meteorol. Soc., 96, 320–325, 1970.

Denman, K. L., Brasseur, G., Chidthaisong, A., Ciais, P., Cox, P. M., Dickinson, R. E., Hauglustaine, D., Heinze, C., Holland, E., Jacob, D., Lohmann, U., Ramachandran, S., da Silva Dias, P. L., Wofsy, S. C., and Zhang, X.: Couplings between changes in the climate system and biogeochemistry, in: Climate Change 2007: The Physical Science Basis. Contribution of Working Group I to the Fourth Assessment Report of the Intergovernmental Panel on Climate Change, edited by: Solomon, S., Qin, D., Manning, M., Chen, Z., Marquis, M., Averyt, K. B., Tignor, M., and Miller, H. L., Cambridge University Press, Cambridge, UK and New York, NY, USA, 499–587, 2007.

Elkins, J. W., Wofsy, S. C., McElroy, M. B., Kolb, C. E., and Kaplan, W. A.: Aquatic sources and sinks for nitrous oxide, Nature, 275, 602–606, 1978.

Forster, G., Upstill-Goddard, R. C., Gist, N., Robinson, C., Uher, G., and Woodward, E. M. S.: Nitrous oxide and methane in the Atlantic Ocean between 50°N and 52°S: latitudinal distribution and sea-to-air flux, Deep-Sea Res. Pt. II, 56, 964–976, doi:10.1016/j.dsr2.2008.12.002, 2009.

OSD
10, 1031–1065, 2013

Forster, P., Ramaswamy, V., Artaxo, P., Berntsen, T., Betts, R., Fahey, D. W., Haywood, J., Lean, J., Lowe, D. C., Myhre, G., Nganga, J., Prinn, R., Raga, G., Schulz, M., and Van Dorland, R.: Changes in atmospheric constituents and radiative forcing, in: Climate Change 2007: The Physical Science Basis. Contribution of Working Group I to the Fourth Assessment Report of the Intergovernmental Panel on Climate Change, edited by: Solomon, S., Qin, D., Manning, M., Chen, Z., Marquis, M., Averyt, K. B., Tignor, M., and Miller, H. L., Cambridge University Press, Cambridge, UK and New York, NY, USA, 2007.

Goreau, T. J., Kaplan, W. A., Wofsy, S. C., McElroy, M. B., Valois, F. W., and Watson, S. W.: Production of NO_2^- and N_2O by nitrifying bacteria at reduced concentrations of oxygen, Appl. Environ. Microb., 40, 526–532, doi:PMCID:PMC291617, 1980.

Gülzow, W., Rehder, G., Schneider, B., Deimling, J. S., and Sadkowiak, B.: A new method for continuous measurement of methane and carbon dioxide in surface waters using off-axis integrated cavity output spectroscopy (ICOS): an example from the Baltic Sea, Limnol. Oceanogr.-Meth., 9, 176–184, 2011.

Juranek, L. W., Hamme, R. C., Kaiser, J., Wanninkhof, R., and Quay, P. D.: Evidence of O_2 consumption in underway seawater lines: implications for air-sea O_2 and CO_2 fluxes, Geophys. Res. Lett., 37, L01601, doi:10.1029/2009GL040423, 2010.

Knowles, R.: Denitrification, Microbiol. Rev., 46, 43–70, 1982.

Liss, P. S. and Merlivat, L.: Air-sea gas exchange rates: introduction and synthesis, in: The role of air-sea exchange in geochemical cycling, editor: Buat-Ménard, Patrick, publisher: Springer Netherlands, doi:10.1007/978-94-009-4738-2_5, ISBN: 978-94-010-8606-6; publishing institution: D. Reidel Publishing Company and place of publication: Dordrecht 185, 113–127, 1986.

Löscher, C. R., Kock, A., Könneke, M., LaRoche, J., Bange, H. W., and Schmitz, R. A.: Production of oceanic nitrous oxide by ammonia-oxidizing archaea, Biogeosciences, 9, 2419–2429, doi:10.5194/bg-9-2419-2012, 2012.

McGillicuddy, D. J., Anderson, L. A., Bates, N. R., Bibby, T., Buesseler, K. O., Carlson, C. A., Davis, C. S., Ewart, C., Falkowski, P. G., and Goldthwait, S. A.: Eddy/wind interactions stimulate extraordinary mid-ocean plankton blooms, Science, 316, 1021–1026, 2007.

McIlvin, M. R. and Casciotti, K. L.: Fully automated system for stable isotopic analyses of dissolved nitrous oxide at natural abundance levels, Limnol. Oceanogr.-Meth., 8, 54–66, 2010.

OSD
10, 1031–1065, 2013

Moore, C. M., Mills, M. M., Achterberg, E. P., Geider, R. J., LaRoche, J., Lucas, M. I., McDonagh, E. L., Pan, X., Poulton, A. J., and Rijkenberg, M. J. A.: Large-scale distribution of Atlantic nitrogen fixation controlled by iron availability, Nat. Geosci., 2, 867–871, 2009.

Nevison, C. D., Weiss, R. F., and Erickson, D. J.: Global oceanic emissions of nitrous oxide, J. Geophys. Res., 100, 15809–15820, 1995.

Nightingale, P. D., Malin, G., Law, C. S., Watson, A. J., Liss, P. S., Liddicoat, M. I., Boutin, J., and Upstill-Goddard, R. C.: In situ evaluation of air-sea gas exchange parameterizations using novel conservative and volatile tracers, Global Biogeochem. Cy., 14, 373–387, 2000.

Oudot, C., Jean-Baptiste, P., Fourrè, E., Mormiche, C., Guevel, M., Ternon, J. F., and Le Corre, P.: Transatlantic equatorial distribution of nitrous oxide and methane, Deep-Sea Res. Pt. I, 49, 1175–1193, 2002.

Popp, B. N., Westley, M. B., Toyoda, S., Miwa, T., Dore, J. E., Yoshida, N., Rust, T. M., Sansone, F. J., Russ, M. E., Ostrom, N. E., and Ostrom, P. H.: Nitrogen and oxygen isotopomeric constraints on the origins and sea-to-air flux of N_2O in the oligotrophic subtropical North Pacific gyre, Global Biogeochem. Cy., 16, 12-1-12-10, doi:10.1029/2001GB001806, 2002.

Poth, M. and Focht, D. D.: ^{15}N kinetic analysis of N_2O production by *Nitrosomonas europaea*: an examination of nitrifier denitrification, Appl. Environ. Microb., 49, 1134–1141, doi:PMCID:PMC238519, 1985.

Prinn, R., Weiss, R., Fraser, P., Simmonds, P., Cunnold, D., Alyea, F., O'Doherty, S., Salameh, P., Miller, B., and Huang, J.: A history of chemically and radiatively important gases in air deduced from ALE/GAGE/AGAGE, J. Geophys. Res.-Atmos., 105, 17751–17792, 2000.

Rafelski, L. E., Paplawsky, B., and Keeling, R. F.: An equilibrator system to measure dissolved oxygen and its isotopes, J. Atmos. Ocean. Tech., 30, 361–377, doi:10.1175/JTECH-D-12-00074.1, 2012.

Ravishankara, A. R., Daniel, J. S., and Portmann, R. W.: Nitrous oxide (N_2O): the dominant ozone-depleting substance emitted in the 21st century, Science, 123–125, doi:10.1126/science.1176985, 2009.

Reuer, M. K., Barnett, B. A., Bender, M. L., Falkowski, P. G., and Hendricks, M. B.: New estimates of Southern Ocean biological production rates from O_2/Ar ratios and the triple isotope composition of O_2, Deep-Sea Res. Pt. I, 54, 951–974, 2007.

OSD
10, 1031–1065, 2013

Rhee, T. S., Kettle, A. J., and Andreae, M. O.: Methane and nitrous oxide emissions from the ocean: a reassessment using basin-wide observations in the Atlantic, J. Geophys. Res., 114, D12304, doi:10.1029/2008JD011662, 2009.

Röckmann, T., Kaiser, J., Brenninkmeijer, C. A. M., and Brand, W. A.: Gas chromatography/isotope-ratio mass spectrometry method for high-precision position-dependent ^{15}N and ^{18}O measurements of atmospheric nitrous oxide, Rapid Commun. Mass Sp., 17, 1897–1908, 10.1002/rcm.1132, 2003.

Suntharalingam, P. and Sarmiento, J. L.: Factors governing the oceanic nitrous oxide distribution: simulations with an ocean general circulation model, Global Biogeochem. Cy., 14, 429–454, 2000.

Sutka, R. L., Ostrom, N. E., Ostrom, P. H., and Phanikumar, M. S.: Stable nitrogen isotope dynamics of dissolved nitrate in a transect from the North Pacific Subtropical Gyre to the Eastern Tropical North Pacific, Geochim. Cosmochim. Ac., 68, 517–527, doi:10.1016/s0016-7037(03)00483-6, 2004.

Sutka, R. L., Ostrom, N. E., Ostrom, P. H., Breznak, J. A., Gandhi, H., Pitt, A. J., and Li, F.: Distinguishing nitrous oxide production from nitrification and denitrification on the basis of isotopomer abundances, Appl. Environ. Microb., 72, 638–644, doi:10.1128/aem.72.1.638-644.2006, 2006.

Walter, S., Bange, H. W., and Wallace, D. W. R.: Nitrous oxide in the surface layer of the tropical North Atlantic Ocean along a west to east transect, Geophys. Res. Lett., 31, L23S07, doi:10.1029/2004GL019937, 2004.

Walter, S., Bange, H. W., Breitenbach, U., and Wallace, D. W. R.: Nitrous oxide in the North Atlantic Ocean, Biogeosciences, 3, 607–619, doi:10.5194/bg-3-607-2006, 2006.

Wanninkhof, R.: Relationship between wind speed and gas exchange, J. Geophys. Res., 97, 7373–7382, 1992.

Weiss, R. F. and Price, B. A.: Nitrous oxide solubility in water and seawater, Mar. Chem., 8, 347–359, 1980.

Weiss, R. F., Van Woy, F. A., and Salameh, P. K.: Surface water and atmospheric carbon dioxide and nitrous oxide observations by shipboard automated gas chromatography: results from expeditions between 1977 and 1990, Oak Ridge National Lab., TN, US, Carbon Dioxide Information Analysis Center, 1992.

OSD
10, 1031–1065, 2013

Wuchter, C., Abbas, B., Coolen, M. J. L., Herfort, L., Van Bleijswijk, J., Timmers, P., Strous, M., Teira, E., Herndl, G. J., and Middelburg, J. J.: Archaeal nitrification in the ocean, P. Natl. Acad. Sci. USA, 103, 12317–12322, doi:10.1073/pnas.0600756103, 2006.

Yoshida, N., Morimoto, H., Hirano, M., Koike, I., Matsuo, S., Wada, E., Saino, T., and Hattori, A.: Nitrification rates and ^{15}N abundances of N_2O and NO_3^- in the western North Pacific, Nature, 341, 895–897, 1989.

Yoshinari, T.: Nitrous oxide in the sea, Mar. Chem., 4, 189–202, 1976.

OSD

10, 1031–1065, 2013

Table 1. Comparison between ICOS and GC-MS measurements during JR255A. Sampling time (GMT) and position for the three depth casts overlapping with analyser measurements. c_{eq} is the equilibrium concentration for atmospheric N_2O based on sea surface temperature (θ_0), salinity (S_0) and atmospheric pressure (p_{atm}).

Date and time	Latitude/ °S	Longitude/ °W	θ_0/ °C	S_0	p_{atm}/ kPa	$c(N_2O, LGR)$/ (nmol L^{-1})	$c(N_2O, GC\text{-}MS)$/ (nmol L^{-1})	$c_{eq}(\theta_0, S_0, p_{atm})$/ (nmol L^{-1})
23 Jan 2012 19:53	63.4	53.0	0.56	34.31	101	15.44 ± 0.02	15.8 ± 0.3	14.9 ± 0.2
24 Jan 2012 03:48	63.5	52.1	0.24	34.02	101	15.36 ± 0.02	15.6 ± 0.3	15.1 ± 0.2
25 Jan 2012 06:35	63.3	53.3	0.46	34.28	100	15.52 ± 0.02	15.6 ± 0.3	15.0 ± 0.2

OSD
10, 1031–1065, 2013

Equilibrator-based measurements of dissolved nitrous oxide

I. Grefe and J. Kaiser

Table 2. Mean N_2O concentration, saturation and air-sea flux for the northern gyre (24–11° N), equatorial region (11° N–5° S, with gaps between 4° N and 2° S) and southern gyre (14–39° S).

	$c(N_2O)$/ ($nmol\,L^{-1}$)	$s(N_2O)$/ (%)	ϕ/ ($\mu mol\,m^{-2}\,d^{-1}$)
24–11° N	5.8 ± 0.1	99.0 ± 1.6	−0.14 ± 0.31
11° N–5° S	5.8 ± 0.2	100.4 ± 1.8	0.11 ± 0.26
14–39° S	7.1 ± 0.7	99.7 ± 1.0	−0.16 ± 0.33

OSD
10, 1031–1065, 2013

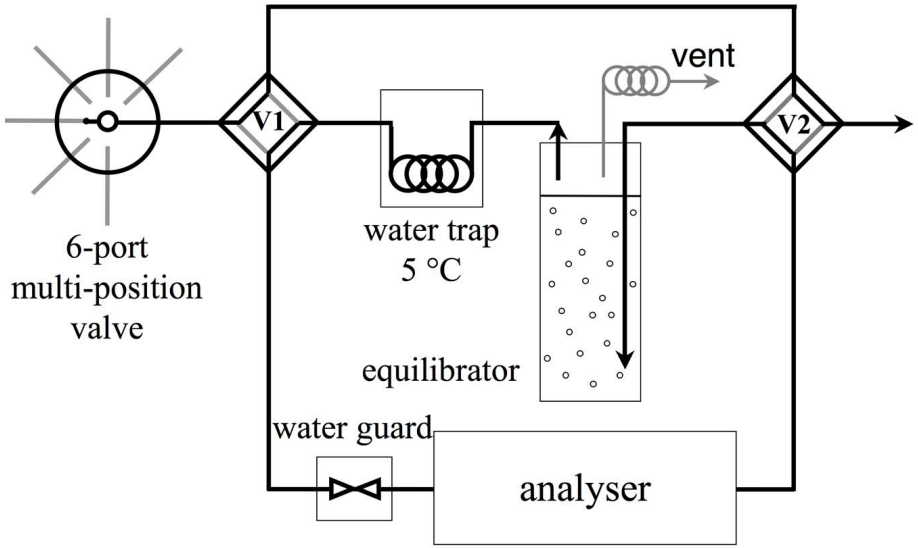

Fig. 1. Setup for laboratory tests. V1 and V2: 4-port 2-position valves. Arrows indicate gas flow through the equilibrator. The vent is a 3 m long coiled 1/8 inch (outer diameter) plastic tube to allow for volume and pressure changes of the equilibrator headspace due to variations in gas tension.

OSD
10, 1031–1065, 2013

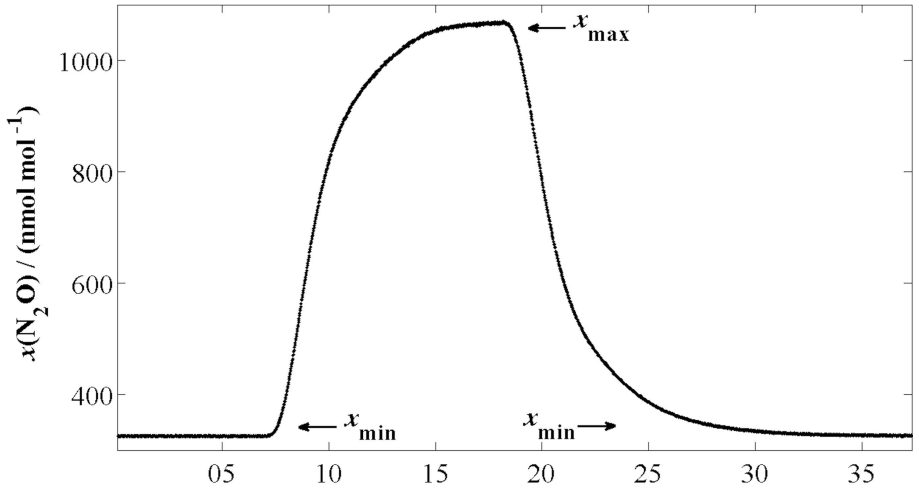

Fig. 2. N_2O mole fractions during step experiment for determination of τ. Equilibrated water flowing through the equilibrator is replaced with water containing higher N_2O concentrations.

OSD
10, 1031–1065, 2013

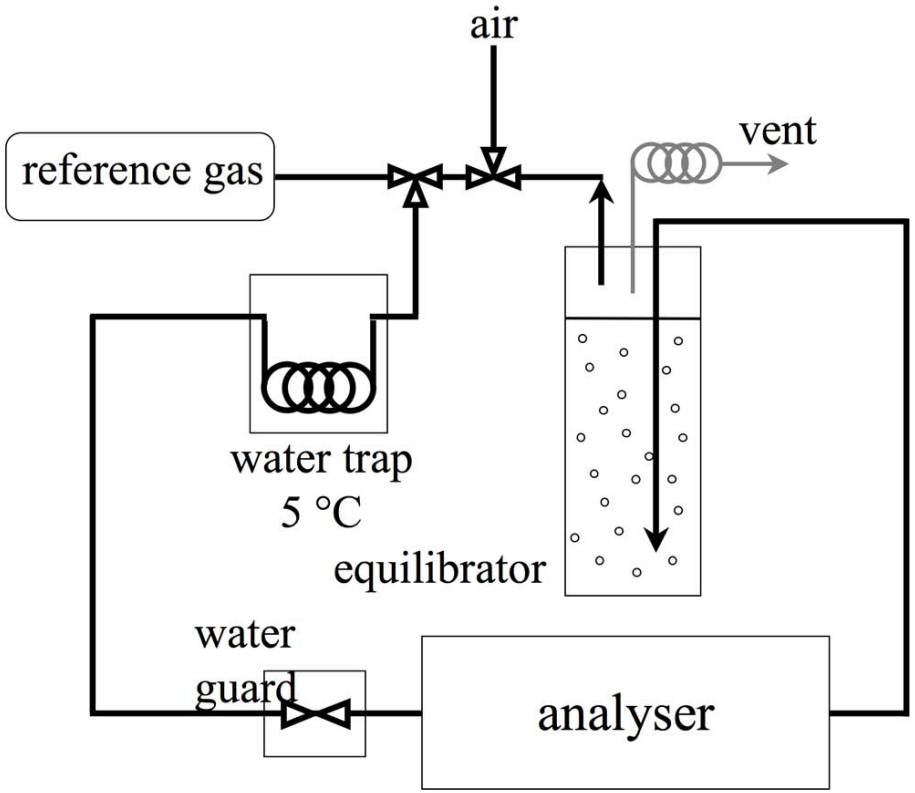

Fig. 3. Underway setup for field deployment during AMT20. Two manual 3-port valves allow switching between measurements of the equilibrator headspace, marine air, and dry air.

OSD
10, 1031–1065, 2013

Equilibrator-based measurements of dissolved nitrous oxide

I. Grefe and J. Kaiser

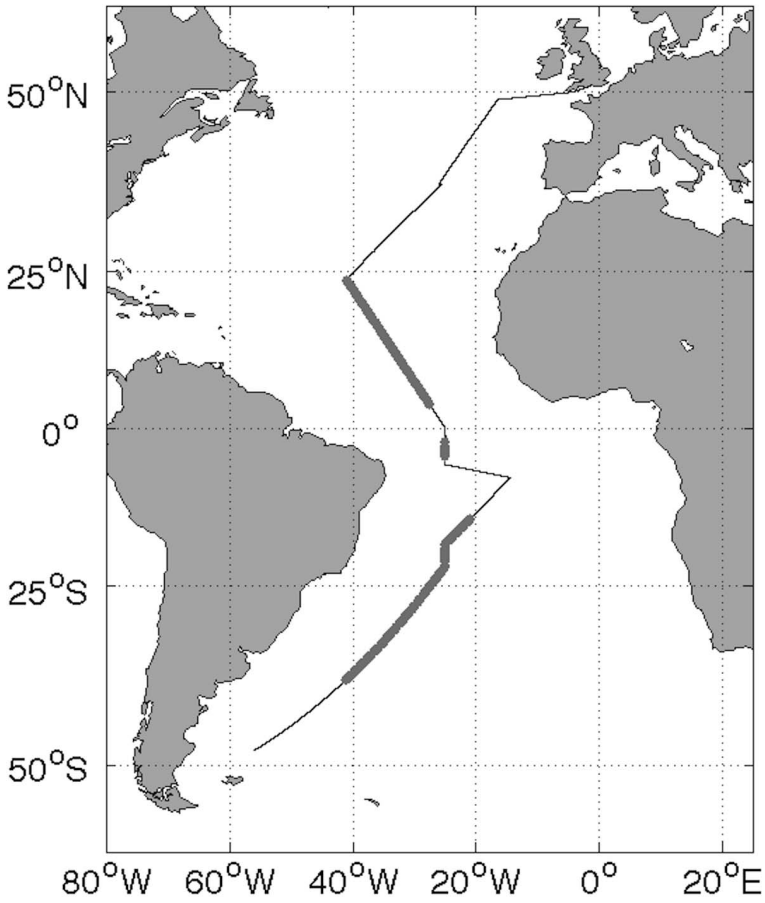

Fig. 4. Cruise track of AMT20. Thick grey lines indicate positions of measurements with the N_2O analyser.

OSD
10, 1031–1065, 2013

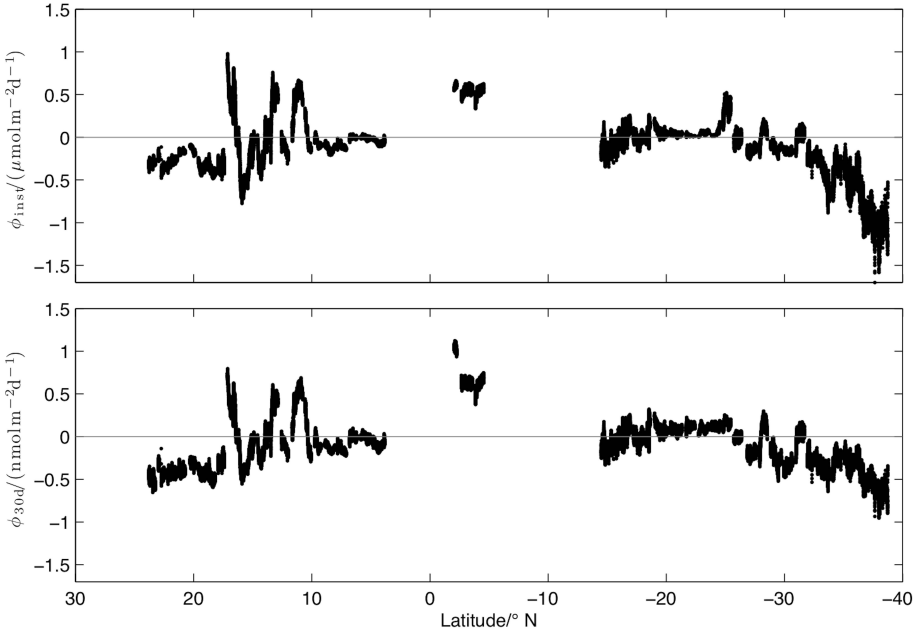

Fig. 5. Comparison of N_2O flux calculated from instantaneous (top panel) and 30 day averaged wind speeds (bottom panel).

OSD
10, 1031–1065, 2013

Equilibrator-based measurements of dissolved nitrous oxide

I. Grefe and J. Kaiser

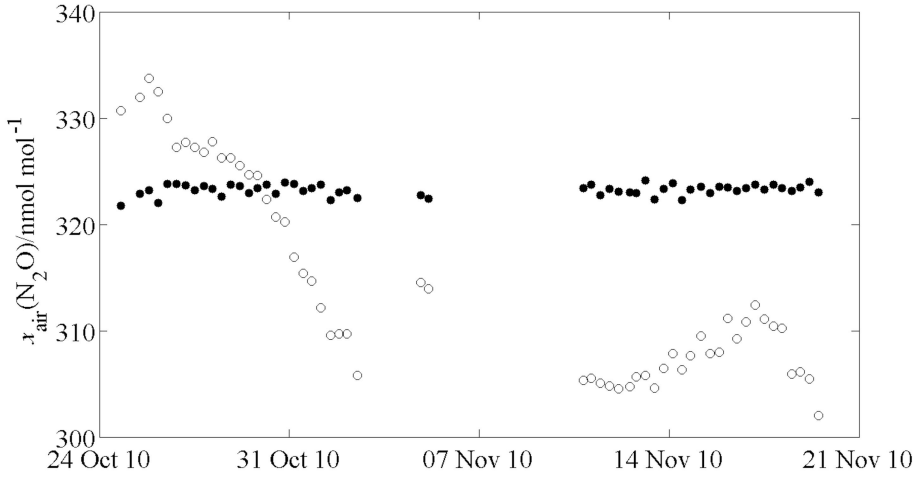

Fig. 6. N_2O mole fractions measured during AMT20 in tropospheric air. Open circles are raw measurement values before drift and offset corrections, filled circles are fully corrected values.

OSD
10, 1031–1065, 2013

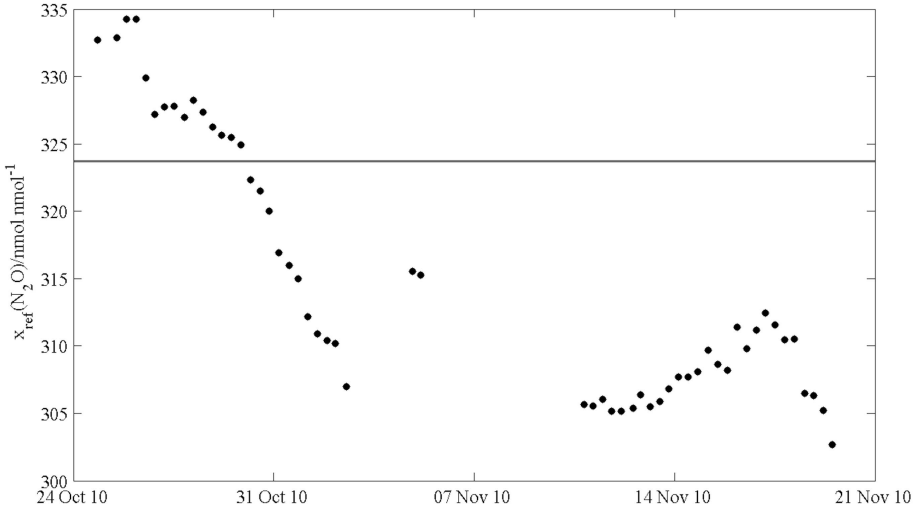

Fig. 7. Measured mole fractions for the reference gas during the transect. Nominal value of 323.7 nmol mol^{-1} indicated by grey line.

OSD
10, 1031–1065, 2013

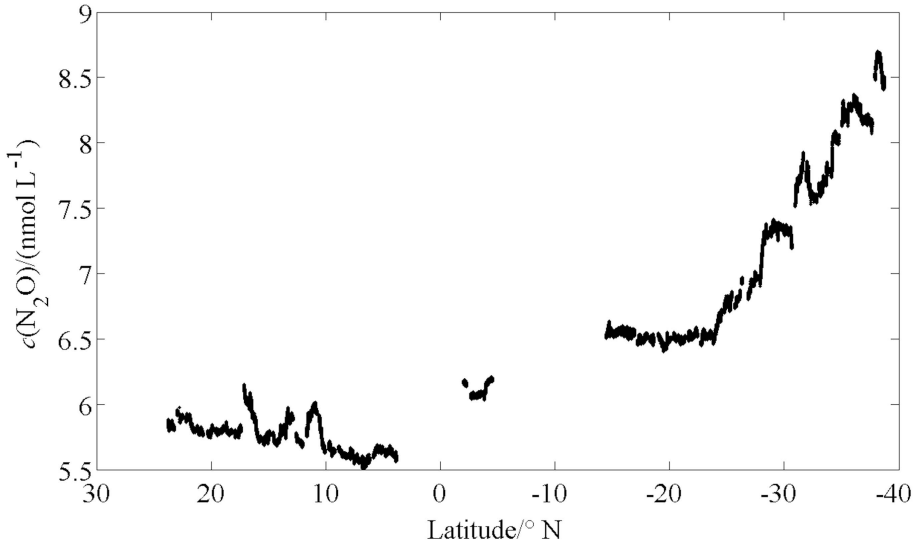

Fig. 8. N_2O concentrations in surface waters during the cruise.

OSD
10, 1031–1065, 2013

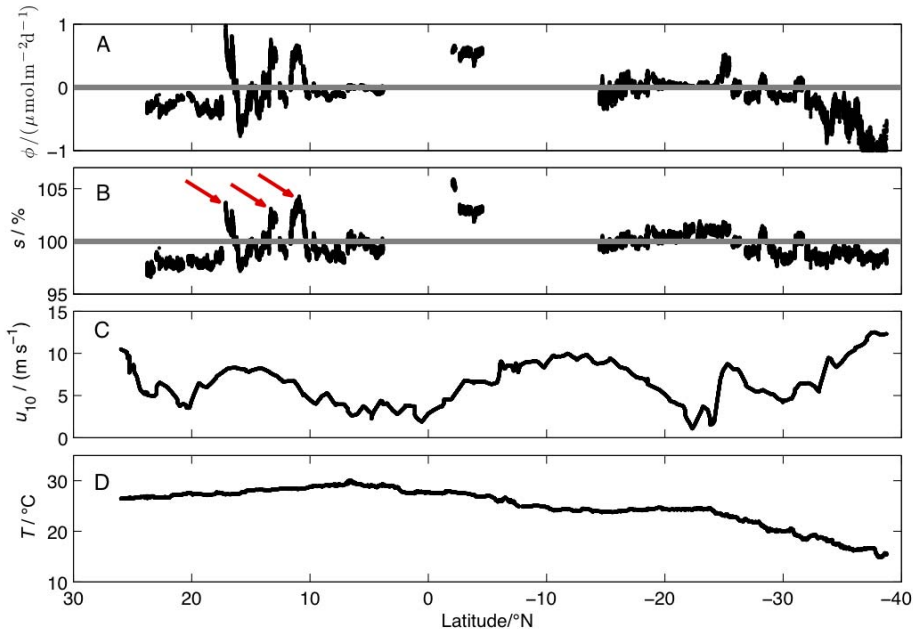

Fig. 9. (A) Sea-to-air N_2O flux, grey line denotes zero flux. Positive values indicate fluxes from sea to air. **(B)** Surface water saturations, equilibrium saturation 100 % indicated by grey line, arrows mark saturation-peaks between 20–10° N (see text for details). **(C)** Wind speed at 10 m height from ECMWF climatology for AMT20. **(D)** Sea surface temperature at inlet.

OSD
10, 1031–1065, 2013

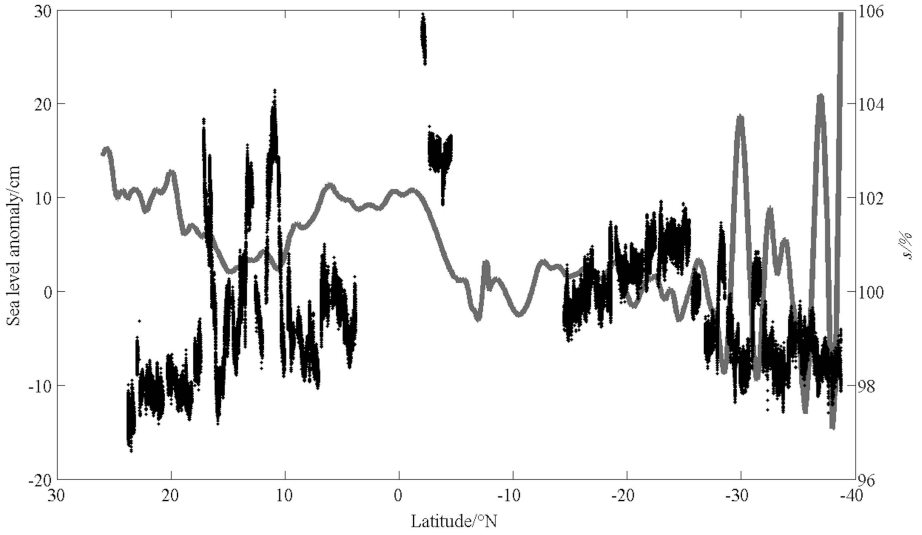

Fig. 10. Meridional variations in sea level height anomaly (grey line, left axis) and N_2O saturation (black dots, right axis).

OSD
10, 1031–1065, 2013

Equilibrator-based measurements of dissolved nitrous oxide

I. Grefe and J. Kaiser